Article

Effects of Anisotropic Thermal Conductivity and Lorentz Force on the Flow and Heat Transfer of a Ferro-Nanofluid in a Magnetic Field

Yubai Li [1], Hongbin Yan [2] ⓘ, Mehrdad Massoudi [3] and Wei-Tao Wu [4],*

[1] Department of Mechanical and Nuclear Engineering, The Pennsylvania State University,
    State College, PA 16803, USA; yxl270@psu.edu
[2] School of Marine Science and Technology, Northwestern Polytechnical University, Xi'an 710072, China;
    hbyan@nwpu.edu.cn
[3] Department of Energy, U. S. National Energy Technology Laboratory (NETL), Pittsburgh, PA 15236, USA;
    mehrdad.massoudi@netl.doe.gov
[4] Department of Biomedical Engineering and Mechanical Engineering, Carnegie Mellon University,
    Pittsburgh, PA 15213, USA
*   Correspondence: weitaow@andrew.cmu.edu; Tel.: +1-412-944-4638

Abstract: In this paper, we study the effects of the Lorentz force and the induced anisotropic thermal conductivity due to a magnetic field on the flow and the heat transfer of a ferro-nanofluid. The ferro-nanofluid is modeled as a single-phase fluid, where the viscosity depends on the concentration of nanoparticles; the thermal conductivity shows anisotropy due to the presence of the nanoparticles and the external magnetic field. The anisotropic thermal conductivity tensor, which depends on the angle of the applied magnetic field, is suggested considering the principle of material frame indifference according to Continuum Mechanics. We study two benchmark problems: the heat conduction between two concentric cylinders as well as the unsteady flow and heat transfer in a rectangular channel with three heated inner cylinders. The governing equations are made dimensionless, and the flow and the heat transfer characteristics of the ferro-nanofluid with different angles of the magnetic field, Hartmann number, Reynolds number and nanoparticles concentration are investigated systematically. The results indicate that the temperature field is strongly influenced by the anisotropic behavior of the nanofluids. In addition, the magnetic field may enhance or deteriorate the heat transfer performance (i.e., the time-spatially averaged Nusselt number) in the rectangular channel depending on the situations.

Keywords: nanofluids; anisotropic thermal conductivity; Lorentz force; magnetic nanofluids (MNFs); heat transfer

1. Introduction

With the rapid development of nanotechnology, various nanofluids have been devised and applied in thermal engineering [1]. Nanofluids are suspensions composed of base fluids and different types of suspending nanoparticles. The base fluids which are commonly used include water, oil, etc. while the nanoparticles are generally made from metals, oxides, carbon nanotubes, graphene, etc. which have higher thermal conductivities. Hence, nanofluids seem to exhibit higher effective thermal conductivity compared to the base fluids; furthermore, based on proper selection and processing of the base fluid and nanoparticles, nanofluids show great performance in a wide range of engineering applications. In heat exchangers, heat sinks, etc. it has been reported that the replacement of convectional working fluids with nanofluids can evidently enhance convective heat transfer with limited increase in pressure drop [1–9].

Due to the outstanding performance and promising engineering applications, especially after the pioneering works by Choi (1995) [10], Eastman et al., (1996) [11], Eastman et al., (2001) [12], Xuan and Li (2000) [13], and Choi et al., (2001) [14], nanofluids have been extensively studied in various problems [2,3,15–18]. For example, Beg et al., (2014) [19] performed a computational fluid dynamics simulation using Al_2O_3–water bio-nanofluids in a circular tube, employing a single-phase model and three different two-phase models (volume of fluid, mixture and Eulerian). The numerical simulations showed that the single-phase and two-phase models predict the same results for fluid flow but different results for thermal fields. Bhatti and Rashidi (2016) [20] studied the combined effects of thermo-diffusion and thermal radiation on Williamson nanofluid over a porous stretching sheet, where physical features for all the pertinent parameters were discussed.

Recently magnetic nanofluids (MNFs) have received some attention, primarily due to their excellent performance in enhancing the heat transfer efficiency; these fluids have been applied in various fields such as chemical engineering, nuclear fusion, medicine and transformer cooling [21,22]. Compared to the conventional nonmagnetic nanofluids, MNFs show several unique features, such as the possibility of controlling the flow or the thermo-physical properties of MNFs using external magnetic fields and providing a more intensive thermo-magnetic convection compared to pure gravitational convection [22]. To investigate these advantages, many studies, focusing on different geometries, have been performed. Zablotsky et al., (2009) [23] presented a study on the thermo-magnetic convection of a magnetic ferro-nanofluid in a rectangular cell under a magnetic field; they found that the heat transfer efficiency is significantly higher than that of the simple thermo-gravitational convection. Xuan et al., (2007) [24] studied the flow and heat transfer in a magnetic ferro-nanofluid flowing through a micro channel using the lattice-Boltzmann method; in their work the effects of the orientation and magnitude of the magnetic field on the fluid flow and heat transfer were included. Rashidi (2016) [25] investigated mixed convective heat transfer of flowing nanofluid in a vertical channel under the effect of a magnetic field. The effects of Grashof number, Reynolds number and Hartman number on Nusslet number and Poiseuille number were systematically studied. For additional information on numerical and experimental investigations on flow and heat transfer of magnetic ferro-nanofluid, see recent review articles [22,26,27].

Usually the thermal conductivity and viscosity of nanofluids is considered to be a function which may depend on the nanoparticles concentration and the properties of the base fluids [13,14,28–30]. According to the review articles [31,32], the thermal conductivity and viscosity usually increase non-linearly in the function of nanoparticle volume concentration. For revealing the mechanism of the thermal and momentum diffusivity of nanofluids and the thermal/dynamic performance at the interface between the fluid and nanoparticles, many works based on experiments [33], theoretical analysis/modelling [6,33] and molecular dynamics simulations [34–37] have been performed. For example, some works indicated that the viscosity of the nanofluids is dependent on the nanoparticles concentration due to the apparently enhanced-viscosity of the base fluid near the solid surface caused by the surface force effects at small scales [29,35,36]. For getting empirical correlations for engineering simulations, many efforts have been made on experimentally measuring the physical properties of nanofluids as well [17,38,39].

For magnetic nanofluids (MNFs), the nanoparticles tend to assemble into chains or rings; as a result, the heat flux along the magnetic field is enhanced dramatically [40]. This indicates that the thermal conductivity of MNFs shows some degree of anisotropy. Recently, this has received some attention, since there is the possibility of controlling the thermal conduction using an external magnetic field [41]. The anisotropic thermal conductivity of MNFs caused by the chain-like aggregation of the ferro-nanoparticles has been investigated by different groups [41–45]. For more information about the theoretical and the experimental studies on the anisotropic thermal conductivity of the magnetic nanofluids, see [46–48].

In this paper, we study the flow and heat transfer in a magnetic nanofluid whose viscosity depends on the volume fraction of the nanoparticles, and thermal conductivity shows anisotropy; the specific

forms of these two transport properties are based on existing experimental data. The transformation of the anisotropic thermal conductivity tensor between different Cartesian coordinate systems is suggested considering the principle of material frame indifference according to Continuum Mechanics. Two specific problems are solved numerically and the results for temperature distributions are discussed for a range of dimensionless numbers.

2. Mathematical Model

In general, under the continuous frame nanofluids can be mathematically modeled by using three different approaches [4,49]: (1) single phase approach where the nanofluid is treated as a conventional single-phase fluid suspension with variable properties; (2) single phase non-homogenous model where the movement of the nanoparticles is modeled by a concentration-flux transport equation [4]; (3) two-fluid approach, such as Mixture theory approach [50–52], where the two components are coupled through interaction forces. In this paper, we consider the nanofluid as a single phase fluid (method 1), where the bulk material properties can depend on the concentration of the particles, applied magnetic field, etc. Compared with the multiphase models, the computational cost of a single phase model is much lower. If the effects of chemical reactions are ignored, the governing equations are the conservation equations for mass, momentum and energy [4,53–56] as detailed below.

2.1. Governing Equations

2.1.1. Conservation of Mass

The conservation of mass reads,

$$\frac{\partial \rho_{nf}}{\partial t} + div\left(\rho_{nf}v\right) = 0 \tag{1}$$

where $\rho_{nf} = (1-\phi)\rho_f + \phi\rho_s = \alpha\rho_f + \phi\rho_s$ is the density of the nanofluid; ϕ and α are the volume fraction (concentration) of the nanoparticles and the base fluid, respectively; ρ_f and ρ_s are the densities of the base fluid and the nanoparticles in the reference configuration (before mixing); $\partial/\partial t$ is the partial derivative with respect to time; and v is the velocity vector. For an incompressible nanofluid [4], the continuum Equation (1) is simplified to,

$$div\ v = 0 \tag{2}$$

2.1.2. Conservation of Linear Momentum

The conservation of linear momentum can be expressed as,

$$\rho_{nf}\frac{dv}{dt} = div\ T + b + F_r \tag{3}$$

where b is the body force, F_r is the Lorentz force, T is the Cauchy stress tensor, and d/dt is the total time derivative given by $d(.)/dt = \partial(.)/\partial t + [grad(.)]v$. The conservation of angular momentum indicates that in the absence of couple stresses the stress tensor is symmetric, i.e., $T = T^{\mathrm{T}}$.

2.1.3. Conservation of Energy

If we ignore thermal radiation, the conservation of energy reads [4,56],

$$\rho_{nf}c_{nf}\frac{d\theta}{dt} = T : L - div\ q + E \cdot J \tag{4}$$

where θ is the temperature, c_{nf} is the specific heat capacity of the nanofluid, T is the stress tensor, L is gradient of the velocity, q is the heat flux vector, $E \cdot J$ is the Joule heating, E is the electric field and J is the current density. In this paper we consider $\rho_{nf}c_{nf} = (1-\phi)\rho_f C_{pf} + \phi\rho_s C_{ps}$, where c_{pf}

and c_{ps} are the specific heat capacity of the pure base fluid and the nanoparticles. The first term on the right hand side of the above equation is the viscous dissipation term. In this paper, we do not consider the entropy inequality (Clausius-Duhem inequality, for details see the book by Liu (2002) [57]). From the above equations, it is clear that constitutive relations are needed for T, F_r, q and $E \cdot J$.

2.2. Constitutive Equations

2.2.1. Stress Tensor

We consider that the nanofluid can be modeled as an incompressible viscous fluid [4,56]; then:

$$T = -pI + \mu_{nf}D \tag{5}$$

where μ_{nf} is the viscosity of the nanofluid, I is the identity tensor, p is the pressure and D is the symmetric part of the velocity gradient. In this paper, we take a water based ferro-nanofluid as the working fluid where the diameter of the Fe_3O_4 nanoparticles is 100 nm. We only consider the effects of the volume fraction (concentration) and assume that the effective shear viscosity can be modeled by the correlation proposed by Sundar et al., (2013) [58] (based on their experimental results):

$$\mu_{nf} = \mu_f \left(1 + \frac{\phi}{12.5}\right)^{6.356} \tag{6}$$

where μ_f is the viscosity of the base fluid. The corresponding kinematic viscosity of the nanofluid can be obtained by $\nu_{nf} = \mu_{nf}/\rho_{nf}$. For a brief review of the viscosity of a suspension/mixture, see [51].

2.2.2. Lorentz Force

For a flowing nanofluid, the Lorentz force is defined as [59,60],

$$F_r = J \times B \tag{7}$$

$$J = \sigma_{nf} v \times B \tag{8}$$

where B is the magnetic induction and σ_{nf} is the effective electrical conductivity of the nanofluid. According to Lagrange's formula, the Lorentz force can further be expressed as,

$$F_r = \sigma_{nf} \cdot (v \times B) \times B = \sigma_{nf}(-v(B \cdot B) + B(B \cdot v)) \tag{9}$$

As indicated by many experiments, the effective electrical conductivity of nanofluids may increase by orders of magnitude by adding a little amount of nanoparticles [61,62]. Previous studies have suggested various models [63–66] for the effective electrical conductivity of nanofluid, but none of them always provides good predictions. Therefore, in this paper, based on the literature review [59–62,67–69], we consider $\sigma_{nf} = 4.0$ S/m (a constant).

2.2.3. Heat Flux Vector

The thermal conductivity of magnetic nanofluids is considered to be anisotropic. The heat flux vector is defined as [70,71],

$$q = -K \nabla \theta \tag{10}$$

where K is the second order anisotropic thermal conductivity tensor. For complex materials, K can also depend on the concentration, the temperature, the shear rate, etc. (see Massoudi (2006) [72,73]). When there is no magnetic field or no nanoparticles present in the fluid, the second order tensor, K, reduces to a scalar and Equation (10) becomes,

$$q = -k \nabla \theta \tag{11}$$

where k is the isotropic thermal conductivity. In general, many nanofluids exhibit anisotropic thermal conductivity due to the chain formation (aggregation) of the nanoparticles [41,42,74], see Figure 1. As a result, K can be given [41,74],

$$K = \begin{bmatrix} k_{||} & 0 & 0 \\ 0 & k_{\perp} & 0 \\ 0 & 0 & k_{\perp} \end{bmatrix} \tag{12}$$

where $k_{||}$ is the thermal conductivity in the direction of the magnetic field and $k_{\perp}$ is the thermal conductivity perpendicular to the direction of the magnetic field (see Fang et al., (2009) [42]). Reinecke et al., (2008) [74] incorporated the Bruggeman's calculation for thermal conductivity of particles chains into Nan's effective medium theory (EMT) [75] for composite materials and suggested the following equations for $k_{||}$ and $k_{\perp}$,

$$k_{||} = k_f\left(\left(1 - \frac{\phi_b}{\phi_{int}}\right) + \left(\frac{\phi_b}{\phi_{int}}\right)(1 - \phi_{int})^{-3}\right) \tag{13}$$

$$k_{\perp} = k_f \frac{(1 - \phi_{int})^{-3} + 1 + \frac{\phi_b}{\phi_{int}}((1 - \phi_{int})^{-3} - 1)}{(1 - \phi_{int})^{-3} + 1 - \frac{\phi_b}{\phi_{int}}((1 - \phi_{int})^{-3} - 1)} \tag{14}$$

where k_f is the thermal conductivity of the base fluid whose thermal diffusivity is defined as $\alpha_f = k_f/\rho_f$, ϕ_b is the bulk-mean volume fraction of the nanoparticles, ϕ_{int} is the volume fraction of the nanoparticles in aggregation due to local magnetic field and is given by [60,76],

$$\phi_{int} = (\phi_m - \phi_h)\tanh(c(\phi_h\xi_e)^2) + \phi_h \tag{15}$$

$$\xi_e = \frac{\mu_0\pi M_s d^3 H}{6k_B T_b} \tag{16}$$

where $\phi_m = 0.638$ is the maximum volume fraction of the magnetic nanoparticles, $\phi_h = \phi_b\left(\frac{\Delta+d}{d}\right)$ is the hydrodynamic volume fraction of the nanoparticles, Δ is the surfactant layer thickness, d is the diameter of the nanoparticles, c is the compression parameter, ξ_e is the effective Langevin parameter, μ_0 is the vacuum permeability, M_s is the saturation magnetization of the nanoparticles, H is the magnetic field intensity, k_B is the Boltzman constant, and T_b is the bulk-mean temperature. The above model has been shown to predict the thermal conductivity of iron-based magnetic nanofluids with various concentrations under saturated magnetic intensities [60].
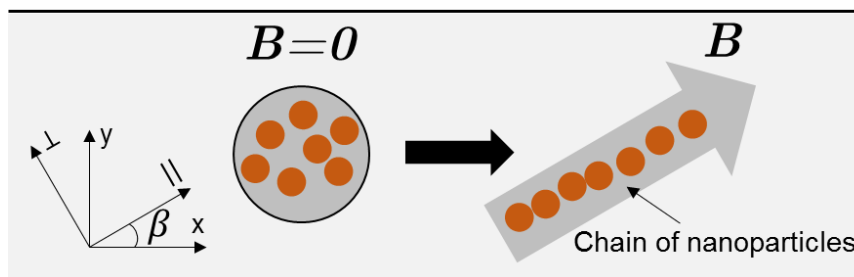

Figure 1. Schematic of the chain formation of nanoparticles. B is the applied uniform magnetic field. $||$ and $\perp$ designate the parallel and the perpendicular directions of the magnetic field, respectively. z-coordinate is perpendicular to the x-y plane.

Equations (13) and (14) provide the thermal conductivity of nanofluids in the directions parallel and perpendicular to the magnetic field; for performing numerical simulations, we need to express the anisotropic thermal conductivity tensor expressed in the x-y-z Cartesian coordinate system. We assume that the anisotropic thermal conductivity caused by the magnetic field is symmetric.

If the applied magnetic field is uniform and always perpendicular to the z-coordinate, then the thermal conductivity tensor in *x-y-z* Cartesian coordinate system can be given by a superposed rigid body rotation of the conductivity tensor $\boldsymbol{K}$ in Equation (12) [77,78],

$$\boldsymbol{K} = \boldsymbol{Q}\boldsymbol{K}\boldsymbol{Q}^{\mathrm{T}} \tag{17}$$

$$\boldsymbol{Q} = \begin{bmatrix} \cos\beta & -\sin\beta & 0 \\ \sin\beta & \cos\beta & 0 \\ 0 & 0 & 1 \end{bmatrix} \tag{18}$$

where $\boldsymbol{Q}$ is an orthogonal tensor (i.e., $\boldsymbol{Q}\boldsymbol{Q}^{\mathrm{T}} = \boldsymbol{Q}^{\mathrm{T}}\boldsymbol{Q} = \boldsymbol{I}$) [77,78], β is the angle between the magnetic field and the *x*-coordinate as shown in Figure 1. The thermal conductivity of the base fluid (water), k_f, at around 300 K is 0.604 W/(m^{-1}·K^{-1}) [79,80]. We should mention that there are studies which also indicate that certain polymers, when sheared, also exhibit anisotropic behavior in their thermal conductivity, see van der Brule (1989) [81] and Dai and Tanner (2006) [82].

2.2.4. Joule Heating

The Joule heating of the nanofluid is given by [59,60],

$$\boldsymbol{E}\cdot\boldsymbol{J} = \sigma_{nf}(\boldsymbol{v}\times\boldsymbol{B})\cdot(\boldsymbol{v}\times\boldsymbol{B}) \tag{19}$$

where $\boldsymbol{E} = \boldsymbol{v}\times\boldsymbol{B}$.

2.3. The Expanded Forms of the Governing Equations and the Boundary Conditions

By substituting Equations (5)–(9) and (9) in Equation (3), and Equations (10)–(19) in Equation (4), we obtain a set of partial differential equations (PDEs) which need to be solved numerically. To obtain numerical solutions to these equations, we build our PDEs solver using the libraries provided by OpenFOAM [83]. The PDEs are given below:

$$div\ \boldsymbol{v} = 0 \tag{20}$$

$$
\begin{aligned}
&\left((1-\phi)\rho_f + \phi\rho_s\right)\left(\frac{\partial \boldsymbol{v}}{\partial t} + (grad\ \boldsymbol{v})\boldsymbol{v}\right) \\
&= -grad\ p + div\left(\mu_f\left(1+\frac{\phi}{12.5}\right)^{6.356}\boldsymbol{D}\right) + \sigma_{nf}(-\boldsymbol{v}(\boldsymbol{B}\cdot\boldsymbol{B}) + \boldsymbol{B}(\boldsymbol{B}\cdot\boldsymbol{v}))
\end{aligned} \tag{21}
$$

$$
\begin{aligned}
&\left((1-\phi)\rho_f C_{pf} + \phi\rho_s C_{ps}\right)\left(\frac{\partial \theta}{\partial t} + (grad\ \theta)\boldsymbol{v}\right) \\
&= \mu_f\left(1+\frac{\phi}{12.5}\right)^{6.356}\boldsymbol{D} : \boldsymbol{L} + \sigma_{nf}|\boldsymbol{v}\times\boldsymbol{B}|^2 + div\ (\boldsymbol{K}\cdot\nabla\theta)
\end{aligned} \tag{22}
$$

The boundary conditions are provided in Table 1. For the velocity at the walls, a no-slip boundary condition is used; for the nanoparticles concentration a no-flux boundary condition ensures that no particle is capable of penetrating the wall. It is worth pointing out that in nanofluidics the hydrodynamic slippage of the fluid is also possible due to the effect of the properties of the interface, such as wettability and roughness [29,35,37,84,85].

Table 1. Boundary conditions used in our numerical simulations. For more details about the boundary conditions, see [86].

Boundary Type	Pressure	Velocity	Concentration	Temperature
Wall	Fixed flux (0)	Fixed value	Fixed flux (0)	Fixed value or flux
Inlet	Fixed value (0)	Fixed value	Fixed value (0)	Fixed value
Outlet	Fixed value (0)	Fixed flux (0)	Fixed flux (0)	Fixed flux (0)

Based on the expanded governing Equations (20)–(22), we define the following non-dimensional parameters:

$$
\begin{aligned}
&X = \tfrac{x}{L_r};\ V = \tfrac{v}{v_0};\ \tau = \tfrac{tv_0}{L_r};\ \overline{\theta} = \tfrac{\theta-\theta_0}{\theta_1-\theta_0};\ P = \tfrac{p}{\rho_f v_0^2};\\
&B^* = \tfrac{B}{B_0};\ X = \tfrac{x}{L_r};\ Y = \tfrac{y}{L_r};\\
&\omega_\rho = \tfrac{\rho_s}{\rho_f};\ \omega_c = \tfrac{C_{ps}}{C_{pf}};\ \omega_k = \tfrac{k_s}{k_f}\\
&\mathrm{div}^*(\cdot) = H\mathrm{div}(\cdot);\ \mathrm{grad}^*(\cdot) = H\mathrm{grad}(\cdot);\ L^* = \mathrm{grad}^* V;\ D^* = \tfrac{1}{2}\left(L^* + L^{*T}\right);\\
&Re = \tfrac{\rho_f v_0 L_r}{\mu_{nf}};\ Ha = L_r B_0 \sqrt{\tfrac{\sigma_{nf}}{\mu_{nf}}};\ D_s = \tfrac{\mu_{nf} v_0}{L_r \rho_s c_{ps}(\theta_1-\theta_0)};\ Le = \tfrac{\kappa_f}{\rho_s c_{ps} v_0 L_r}
\end{aligned}
\tag{23}
$$

where L_r is a reference length, v_0 is a reference velocity, θ_1 and θ_0 are reference temperatures and are chosen as the temperature of the hot wall and the inlet boundary, respectively. B_0 is the reference magnitude of the magnetic field and is chosen as the magnitude of the applied magnetic field. Re is the Reynolds number, Ha is the Hartmann number which is the ratio of electromagnetic force to the viscous force, Le is the Lewis number which is the ratio of thermal diffusivity to convective mass transport and D_s is the dimensionless number related to the viscous dissipation. In the following studies, the heat (viscous) dissipation is ignored, i.e., we assume $D_s = 0$. With the above dimensionless numbers/variables, the governing equations can be written as,

$$
div\ V = 0
\tag{24}
$$

$$
((1-\phi) + \phi\omega_\rho)\left(\frac{\partial V}{\partial \tau} + (grad\ V)V\right) = -grad\ P + \frac{1}{Re}div(D) + Ha^2\frac{1}{Re}(-V(B\cdot B) + B(B\cdot V))
\tag{25}
$$

$$
\left(\frac{(1-\phi)}{\omega_\rho\omega_c} + \phi\right)\left(\frac{\partial\overline{\theta}}{\partial\tau} + (grad\ \overline{\theta})V\right) = Ha^2 D_s|V\times B|^2 + Le\left(div\left(\frac{K}{k_f}\cdot\nabla\overline{\theta}\right)\right)
\tag{26}
$$

In the above equations, the asterisks have been dropped for simplicity. We further define the Nusselt number which is a measure of the ratio of the convective to the conductive heat transfer across (normal to) the boundary. The local Nusselt number is defined as,

$$
Nu = -\left.\frac{\partial\overline{\theta}}{\partial n}\right|_w
\tag{27}
$$

The spatially averaged Nusselt number is defined as (see Wu et al., (2017) [87]),

$$
\overline{Nu}_s = \frac{1}{L}\int_0^L Nu\ ds
\tag{28}
$$

And the time and the spatially averaged Nusselt number is defined as,

$$
\overline{Nu}_{st} = \frac{1}{t_1-t_0}\int_{t_0}^{t_1}\overline{Nu}_s\ dt
\tag{29}
$$

We should mention that in this paper, we do not consider the effect of turbulence because of the low Reynolds number studied.

3. Physical Problems

In this paper, we study two different problems. The first one is a (pure) conduction problem between two concentric cylinders as shown in Figure 2a. In this case, we ignore the flow and focus on the mechanism and the effects of the magnetic field-induced anisotropic thermal conductivity. We assume that the initial temperature is 300 K, while the temperatures of the inner and the outer cylinders are 310 K and 300 K, respectively. The effect of the angle of the magnetic field and the nanoparticles concentration on the anisotropic thermal conductivity and the temperature

distribution are studied. The second problem is an unsteady two-dimensional flow in a rectangular channel over three heated cylinders; see Figure 2b. This kind of a flow is an example of the cross-flow heat exchanger which is common in engineering applications. We study the flow and heat transfer of the nanofluid with different Hartmann numbers and angles of the magnetic field. The inlet temperature and the initial temperature are set at 300 K, while the temperature of the inner cylinder is set at 310 K. Other walls are adiabatic. The thermo-physical properties of the nanofluid are summarized in Table 2.
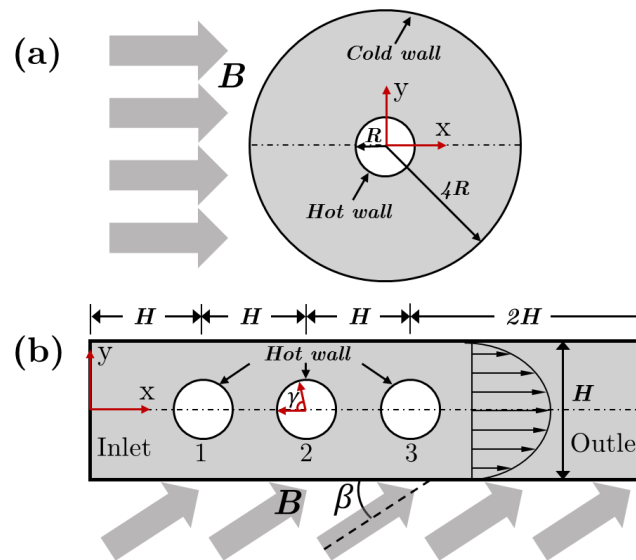
Figure 2. Illustration of the two physical problems: (**a**) heat conduction of a stationary nanofluid situated between two concentric cylinders; (**b**) unsteady flow over three cylinders in a rectangular channel. For both problems, a uniform external magnetic field is applied.

Table 2. Physical properties of the water based Fe_3O_4 nanofluid studied in the present study.

Physical Property	Value	Physical Property	Value
ρ_{f0}	1000 kg/m^3 [88,89]	k_{f0}	0.604 W/(m·K) [79,80]
ρ_{s0}	5180 kg/m^3 [59]	M_s	39 A·m^2/kg [60,76]
d_p	100 nm [90]	c	10 [60,76]
μ_f	1.0 cP [88,89]	Δ	2 nm [60,76]
c_{pf0}	4180 J/(kg·K) [88,89]	μ_0	1.256×10^{-6} N/A^2
c_{ps0}	670 J/(kg·K) [58,59]	k_B	1.381×10^{-23} J/K

For both geometries, a mesh dependency study is performed, but we only show the details for the second problem. To consider the mesh dependency, we use $\overline{\phi} = 0.01$, $Ha = 0$, $Re = 1000$ and $Le = 0.0001$. Table 3 shows the time and spatially averaged Nusselt number, $\overline{Nu}_{st}$, with different mesh sizes. The mesh node numbers of 32,514 and 40,130 almost give the same value for the $\overline{Nu}_{st}$ (less than 0.13%); therefore, we use the mesh with node number of 40,130.

Table 3. Time-spatially averaged Nusselt number, $\overline{Nu}_{st}$, with different meshes for the rectangular channel with three inner cylinders.

Mesh Size	$\overline{Nu}_{st}$	Mesh Size	$\overline{Nu}_{st}$
13,944	93.82	32,514	91.03
23,468	91.46	40,130	90.91

4. Results and Discussion

4.1. Heat Conduction between Two Concentric Cylinders

In this section, the radius of the outer cylinder is chosen as the reference length, L_r. The Hartmann number is assumed to be $Ha = 1.0$. We define a dimensionless time for this pure conduction problem,

$$\tau = \frac{t\alpha_f}{L_r} \tag{30}$$

where α_f is the thermal diffusivity of the base fluid. Table 4 shows the value of the thermal conductivity of the nanofluid in parallel and perpendicular directions to the magnetic field with different nanoparticles concentrations. As the concentration increases, the thermal conductivity begins to show more anisotropy. When the nanoparticles concentration is 0.1, the thermal conductivity in the direction of the magnetic field is about 3 times that of the thermal conductivity perpendicular to the magnetic field. Of course, the anisotropy disappears when the nanoparticle concentration reduces to be zero.

Table 4. The values of the thermal conductivity of the nanofluid paralell and perpendicular to the magnetic field with different nanoparticles concentrations.

$\overline{\phi}$	$k_{||}$ $(W/(m{\cdot}k))$	$k_{\perp}$ $(W/(m{\cdot}k))$
0.0	0.604	0.604
0.005	0.616	0.613
0.01	0.672	0.624
0.02	0.981	0.640
0.05	1.555	0.697
0.1	2.505	0.805

Figure 3 shows the temperature distribution as a function of time. The nanoparticles concentration and the direction of the magnetic field are chosen as $\overline{\phi} = 0.05$ and $\beta = 0°$ (parallel to the X-direction), respectively. From Figure 3a, we can see that as time (τ) increases, heat transfer occurs from the inner hot cylinder to the outer cooler cylinder. The temperature field does not seems to develop in a symmetric way and it appears to have an elliptical pattern due to the effect of the anisotropic thermal conductivity; along the magnetic field the heat conduction occurs at a faster rate. In Figure 3b, we quantitatively elucidate this phenomenon by plotting the temperature profiles along the X and Y directions (radial direction).
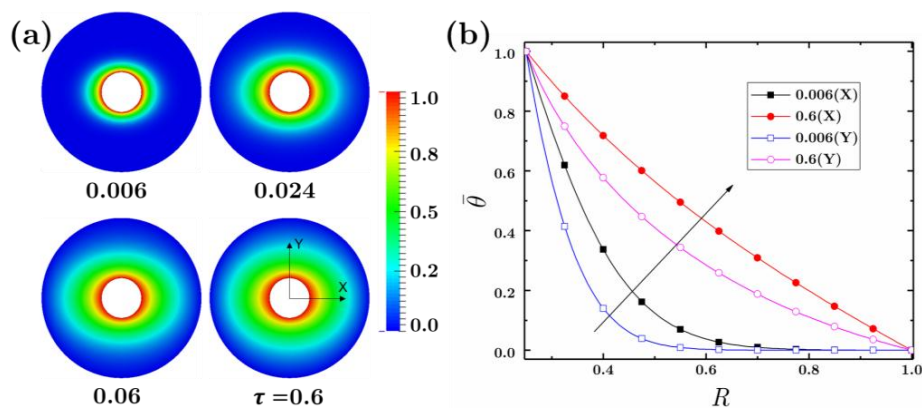

Figure 3. Transeint thermal behavior of the nanofluid at $Ha = 1.0$, $\overline{\phi} = 0.05$ and $\beta = 0°$: (**a**) time evolution of the temperature field between two concentric cylinders; (**b**) temperature profiles along X and Y directions at two different dimensionless time (τ).

In Figure 4, we change the angle of the magnetic field (β) and consider its effect on the temperature distribution. The nanoparticles concentration, $\bar{\phi}$, is kept at 0.05. Figure 4a shows the variation of the steady-state temperature field with β; we can see that as β changes, the temperature distribution is affected considerable, where the fastest heat conduction occurs along the direction of the magnetic field. Figure 4b,c present the temperature profiles in the parallel and the perpendicular direction to the magnetic field with different values of β for four different dimensionless time; it can be seen that the profiles at the same dimensionless time exactly overlap with each other.
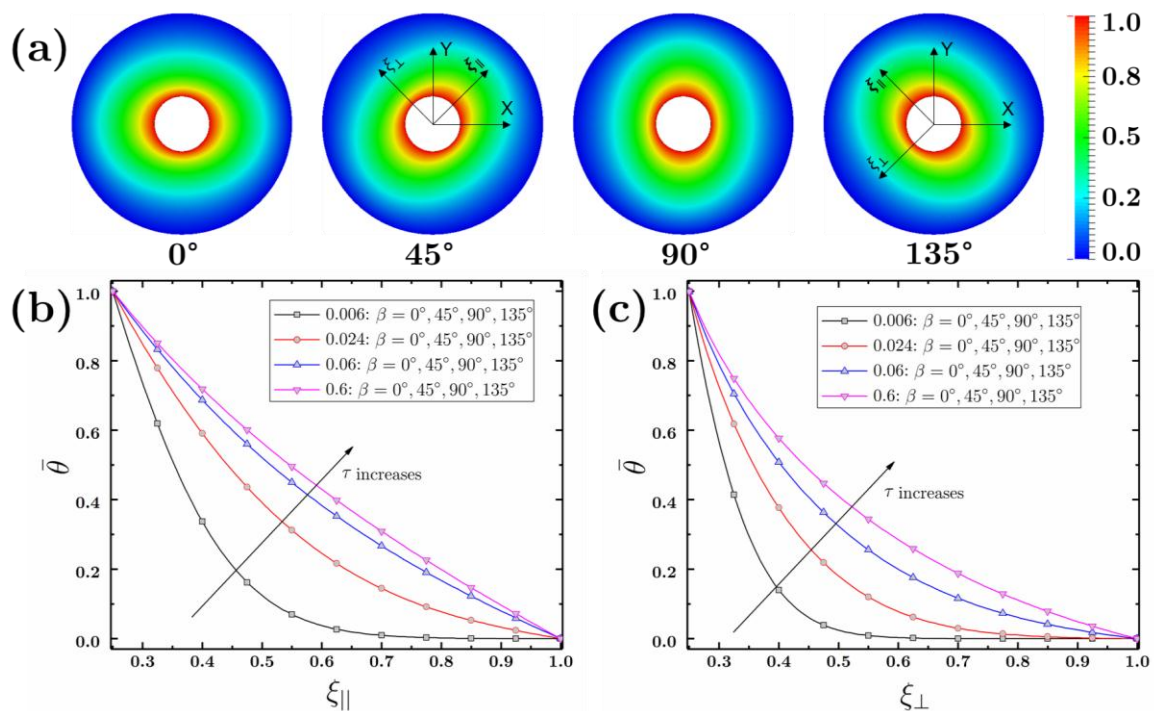

Figure 4. The effect of changing the direction of the magnetic field on thermal bahavior at $Ha = 1.0$ and $\bar{\phi} = 0.05$: (**a**) steady-state temperature distribution; (**b**) temperature profiles along the direction of the magnetic field at different dimensionless times; (**c**) temperature profiles perpendicular to the direction of the magnetic field at different dimensionless times.

Figure 5 shows the effect of the nanoparticles concentration on the non-uniform heat conduction. As shown in Table 4, when the nanoparticles concentration increases, the anisotropy of the thermal conductivity of the nanofluid becomes more evident. The effect of the intensified anisotropic thermal conductivity on the temperature distribution is shown in Figure 5a. When $\bar{\phi} = 0$, the heat conduction is uniform along the radial direction; as $\bar{\phi}$ increases, the temperature distribution becomes more and more non-uniform. Figure 5b,c quantitatively show the steady-state temperature profiles along the X ($\xi_{\parallel}$) and the Y ($\xi_{\perp}$) directions, from which we can observe the effect of $\bar{\phi}$ on the heat transfer.
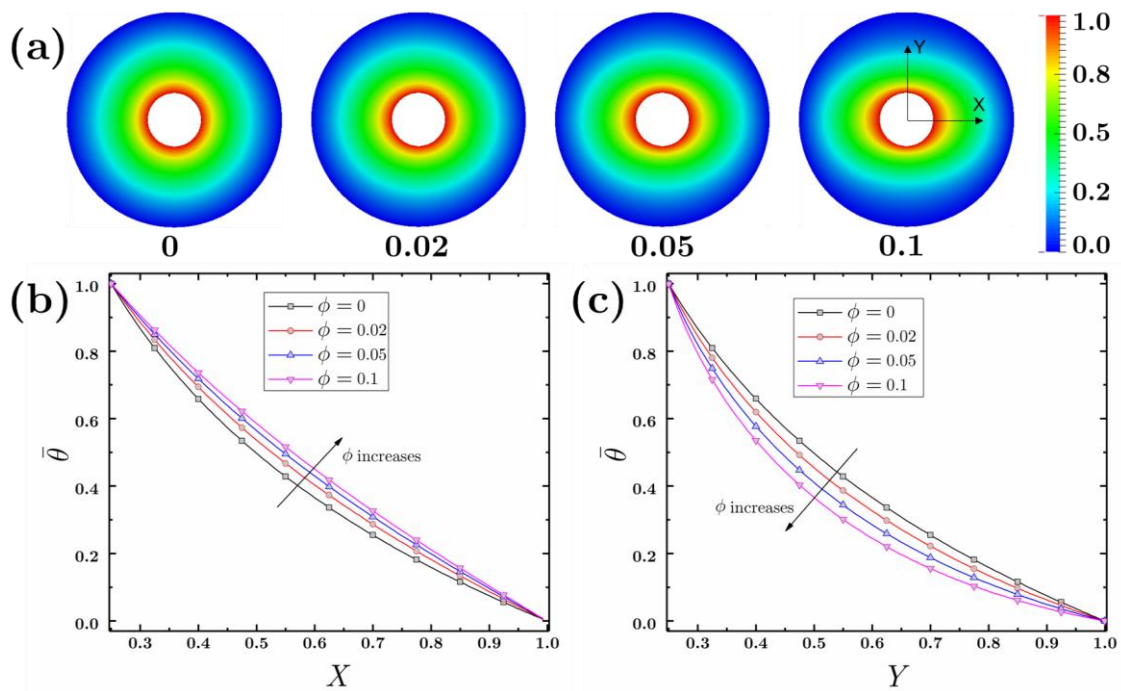
Figure 5. Effect of nanoparticles concentration ($\overline{\phi}$) on (**a**) steady-state temperature distribution; (**b**) steady-state temperature profiles along the *X*-direction; and (**c**) steady-state temperature profiles along the *Y*-direction. For this figure, $Ha = 1.0$ and $\beta = 0°$.

4.2. Flow in A Rectangular Channel with Multiple Cylinders

In this section, the hydraulic diameter at the inlet of the channel is chosen as the reference length, L_r. The concentration of the nanoparticles is assumed to be $\overline{\phi} = 0.01$ for all the following studies. In this section, we focus on two problems: (**a**) when the Reynolds number and the Hartmann number are relatively low; (**b**) when the Reynolds number and the Hartmann number are relatively high.

4.2.1. Flow at Low Reynolds Number

We first study the case with low Reynolds number and low Hartmann number, which is commonly found in heat exchangers applications in micro cooling systems in small electronic devices. In this study, we assume $Re = 1.0$ and $Le = 0.03$.

Figure 6a shows the steady-state velocity and the Lorentz force distributions when $Ha = 0.4$ and $\beta = 90°$. We can see that the Lorentz force always acts in the opposite direction to the main flow, which implies that the Lorentz force has a tendency to impede the flow. Figure 6b,c shows the effect of the Hartmann number, Ha, on the flow and heat transfer, with the angle of the magnetic field $\beta = 90°$. Figure 6b shows that the temperature distribution varies moderately with different values of Ha. In the wake region of the inside cylinders, as Ha increases the size of the thermal boundary layer decreases to some extent; as a result, the heat transfer may be improved and the time and spatially averaged Nusselt number, $\overline{Nu}_{st}$, may increase as shown in Table 5 (left). Figure 6c shows the local Nusselt number (Nu) distribution along the angular coordinates (γ) of the three inner cylinders. For the definition of γ, see Figure 2b. We can see that Nu profile is almost symmetric along γ, because we have assumed a low Reynolds number and there is no vortex in the wake region. Nu is relatively high at $\gamma = 0°$ or $\gamma = 90°$, because the position of $\gamma = 0°$ corresponds to the leading edge and with $\gamma = 90°$ the channel becomes narrow. Hence in these two positions the heat convection is relatively high.
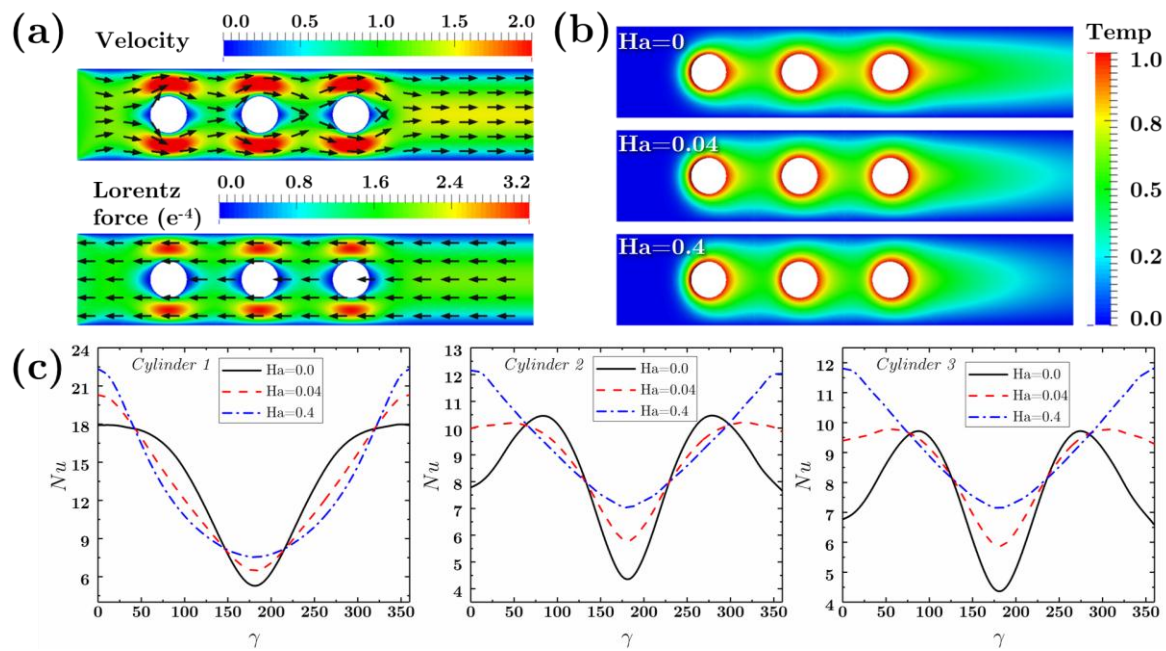
Figure 6. (**a**) The steady-state velocity and the Lorentz force distribution when $Ha = 0.4$; (**b**) effect of the Hartmann number (Ha) on temperature distribution; (**c**) effect of the Hartmann number (Ha) on the local Nussel number distribution along inner cylinder 1, 2 and 3, when $\overline{\phi} = 0.01$, $\beta = 90°$, $Re = 1.0$ and $Le = 0.03$.

Table 5. Effect of Hartmann number (Ha) and the angle of magnetic field (β) on time and spatically averaged Nusselt number ($\overline{Nu}_{st}$).

Ha	$\overline{Nu}_{st}$	**fi(°)**	$\overline{Nu}_{st}$
0	9.91	0	8.21
0.04	10.21	45	9.04
0.4	10.55	90	10.55

Figure 7 shows the effect of the direction of the magnetic field, β, where we assume $Ha = 0.4$. Figure 7a shows the Lorentz force distributions for different values of β. When $\beta = 0°$, the Lorentz force is perpendicular to the direction of the main flow and its magnitude is small. When $\beta = 0°$, the direction of the magnetic field is the same as that of the main flow; according to Equation (9), therefore, the Lorentz forces disappears if the velocity is parallel to the magnetic field. As a result, the magnitude of the Lorentz force increases as β changes from $0°$ to $90°$. Figure 7b indicates that as β increases from $0°$ to $90°$, the thermal boundary layer decreases obviously, see the case of $\beta = 0°$ and $\beta = 45°$ for example. Figure 7c shows the Nu profiles along the angular coordinate of the cylinders; the pattern is similar to those in Figure 6c. Table 5 (right) shows that $\overline{Nu}_{st}$ increases as β changes from $0°$ to $90°$, when the magnitude of the Lorentz force increases.
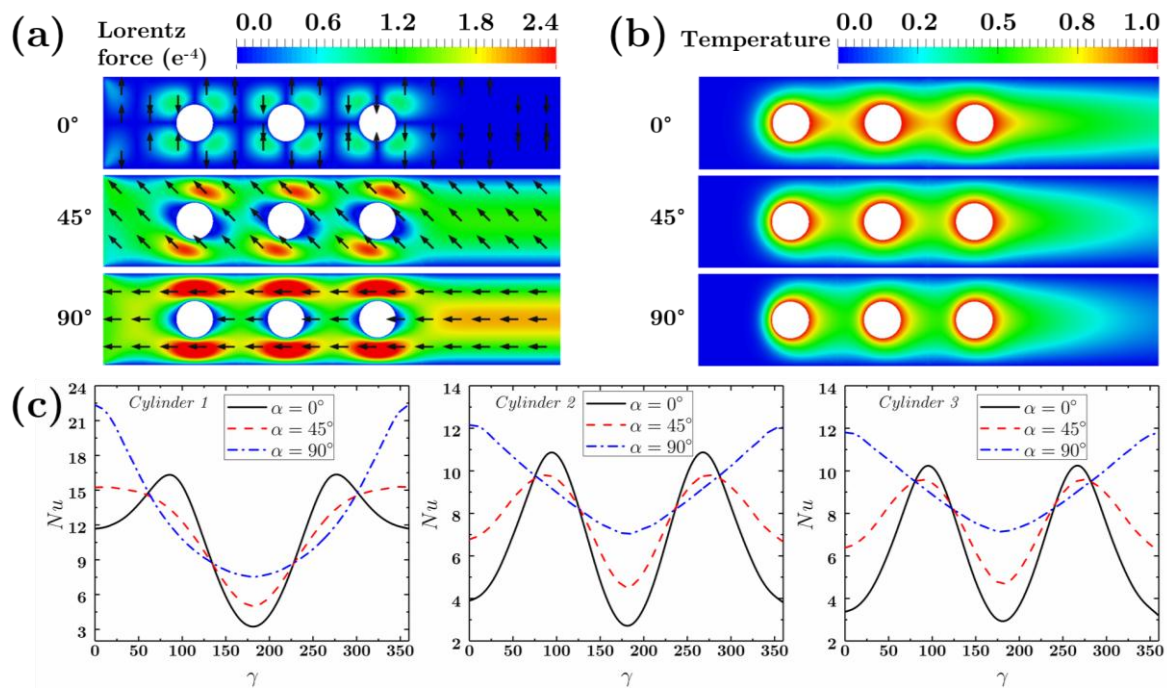
Figure 7. Effect of the angle of magnetic field (β) on (**a**) Lorentz force field; (**b**) temperature field; and (**c**) local Nusselt number distribution along the circumference of the inner cylinder 1, 2 and 3, resepctively. For this figure, $\overline{\phi} = 0.01$, $Re = 1.0$, $Ha = 0.4$ and $Le = 0.03$.

4.2.2. Flow at High Reynolds Number

As the size of the heat exchanger increases, the value of the Re and Ha also usually increase. Therefore, we consider situations with high Re and Ha. We assume $Re = 1000$ and $Le = 0.0001$. Figure 8a,b presents the temperature and the velocity distributions for different values of Ha and β. We can see that when $Ha = 0$, namely where there is no magnetic field, in the wake region after the third cylinder, vortices are developed; while when $Ha = 50$, there are no vortices for both cases of $\beta = 0°$ and $\beta = 90°$. Furthermore, for the temperature fields, if we compare the cases of $\beta = 0°$ and $\beta = 90°$, the size of the thermal boundary layer decreases when $\beta = 90°$. Figure 8d shows the time evolution of the spatially averaged Nusselt number, $\overline{Nu}_s$, for the three cylinders. At the initial stage, $\overline{Nu}_s$ is high and then it begins to decrease rapidly as time increases. Figure 8d also shows the small sinusoidal oscillation of $\overline{Nu}_s$ for the case of $Ha = 0$, when the flow reaches semi-steady state. Figure 8e shows the effect of Ha and β (0°~90°) on $\overline{Nu}_{st}$. When Ha is small (5, 25), $\overline{Nu}_{st}$ decreases moderately as β increases; when Ha is large (50, 100), $\overline{Nu}_{st}$ increases as β increases. The decreasing of $\overline{Nu}_{st}$ may can be attributed to the reduction of the flow disturbance (flow oscillation after the cylinders) when the magnetic field is applied, see cases of $Ha = 0$, $\beta = 0°$ and $Ha = 50$, $\beta = 0°$ in Figure 8a,c. The increasing of $\overline{Nu}_{st}$ may be attributed to the reduction of the size of the wake region after the cylinders where the heat convection is low and, when the Lorentz forces (Ha) is large (see cases of $Ha = 50$, $\beta = 0°$ and $Ha = 50$, $\beta = 90°$ in Figure 8a,c). The effect of the magnetic field on the flow and heat transfer is more complicated; it may reduce or deteriorate the heat transfer in nanofluids depending on the situations. The effect of the enhancement [23,60] and the suppression [91,92] of the magnetic field has been indicated by previous studies.
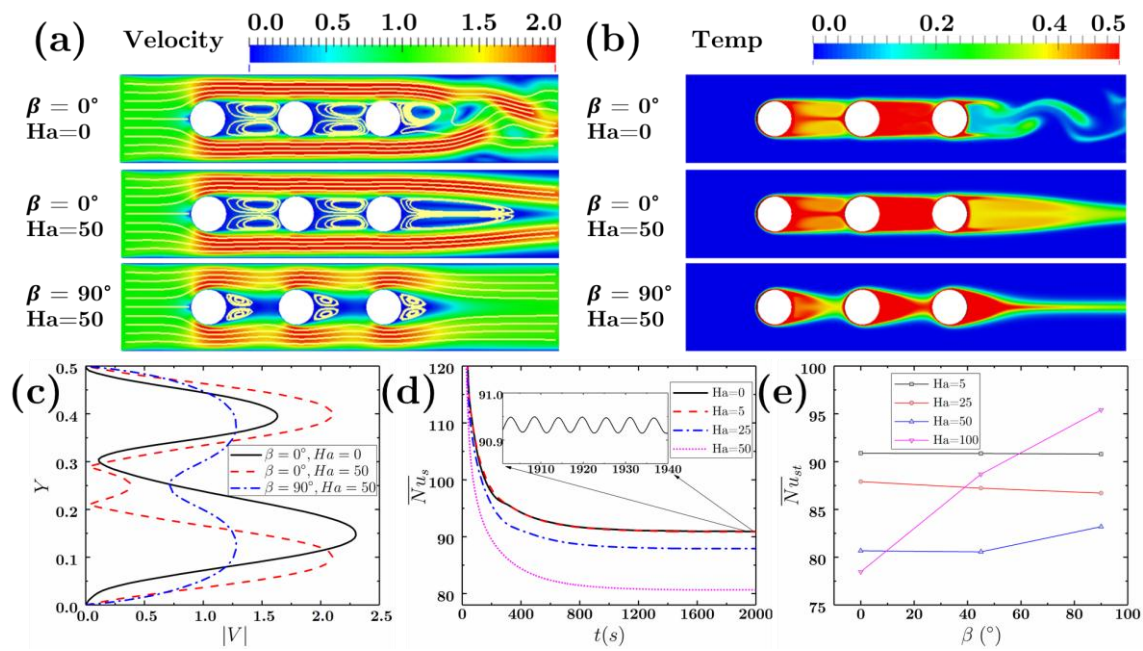
Figure 8. Effect of the Hartmann number (*Ha*) and the angle of the magnetic field (*β*) on (**a**) velocity and (**b**) temperature fields; (**c**) Effect of *Ha* and *β* on dimensionless velocity profiles distribution along Y direction at X = 4; (**d**) Time evolution of spatially averaged Nusselt number, $\overline{Nu_s}$, of three cylinders; (**e**) Effect of *Ha* and *β* on spatial and time averaged Nusselt number, $\overline{Nu_{st}}$. For this figure, $\overline{\phi} = 0.01$, *Re* = 1000 and *Le* = 0.0001.

5. Conclusions

In this paper, we have studied the effect of the magnetic field induced anisotropy of the thermal conductivity of a ferro-nanofluid and the Lorentz force on the flow and heat transfer. We have considered two cases: pure conduction in a stationary nanofluid contained between two concentric cylinders and the unsteady flow and heat transfer in a rectangular channel with three heated cylinders. The numerical results indicate that there is a significant effect on the heat conduction due to the anisotropic nature of the thermal conductivity: the temperature fields appear to be elliptical, because the intensity of the heat conduction in the direction and perpendicular to the magnetic field differs greatly. For the problem of the unsteady flow and heat transfer, it was observed that with the application of the magnetic field, vortices in the wake region behind the cylinders were suppressed, and the flow becomes more stable.

Author Contributions: Yubai Li and Wei-Tao Wu did all the numerical simulations. Wei-Tao Wu, Hongbin Yan and Mehrdad Massoudi derived all the equations. Mehrdad Massoudi supervised this work. All of the authors have provided substantial contributions to the manuscript preparation.

Conflicts of Interest: The authors declare no conflict of interest.

Nomenclature

b	body force vector (N/kg)	***V***	dimensionless velocity vector
F_r	Lorentz force (N)	*Re*	Reynolds number
c_{pf}	specific heat of pure fluid (J/(kgK))	***T***	stress tensor (Pa)
c_{nf}	specific heat of nanofluid (J/(kgK))	v_0	reference velocity (m/s)
C_{ps}	specific heat of pure nanoparticles (J/(kgK))	***v***	velocity vector (m/s)
d_p	diameter of nanoparticles (m)	V_0	mean inlet velocity (m/s)
D	symmetric part of velocity gradient (s^{-1})	***x***	position vector (m)

D_T	diffusivity tensor of thermophoresis (m^2/s)	X, Y	dimensionless Cartesian coordinates
E	electric field (V/m)		
J	current density (A/m^2)	Greek symbols	
B	magnetic field (T)	α	volume fraction of base fluid
K	thermal conductivity tensor (W/(mK))	α_f	thermal diffusivity of base fluid (m^2/s)
L_r, H	reference length scale, height of inlet channel (m)	θ	temperature (K)
k_B	Boltzmann constant (J/K)	$\theta_r, \theta_0, \theta_1$	reference temperatures (K)
k_f	thermal conductivity of pure fluid (W/(mK))	$\theta^*, \bar{\theta}$	dimensionless temperature
k_{nf}	thermal conductivity of nanofluid (W/(mK))	μ_f	dynamic viscosity of base fluid (Pa·s)
k_p	thrmal conductivity of particles (W/(mK))	μ_{nf}	dynamic viscosity of nanofluid (Pa·s)
L	Velocity gradient (s^{-1})	ν_{nf}	kinematic viscosity of nanofluid (m^2/s)
Nu	local Nusselt number	ρ_f	density of base fluid (kg/m^3)
$\overline{Nu}_s$	Spatially averaged Nusselt number	ρ_{nf}	density of nanofluid (kg/m^3)
$\overline{Nu}_{st}$	time and spatially averaged Nusselt number	ρ_s	density of pure nanoparticles (kg/m^3)
p	pressure (Pa)	τ	dimensionless time
t	time	ϕ	volume fraction of nanoparticles
Ha	Hartmann number	σ_{nf}	electrical conductivity of nanofluids (S/m)
Le	Lewis number	ω_ρ	ratio of density
D_s	viscous dissipation dimensionless number	ω_c	ratio of specific heat capacity
q	heat flux vector (W/m^2)	ω_k	ratio of thermal conductivity

References

1. Li, Q.; Xuan, Y.; Wang, J. Investigation on convective heat transfer and flow features of nanofluids. *J. Heat Transf.* **2003**, *125*, 151–155.
2. Safaei, M.R.; Ahmadi, G.; Goodarzi, M.S.; Safdari Shadloo, M.; Goshayeshi, H.R.; Dahari, M. Heat transfer and pressure drop in fully developed turbulent flows of graphene nanoplatelets–silver/water nanofluids. *Fluids* **2016**, *1*, 20. [CrossRef]
3. Safaei, M.R.; Ahmadi, G.; Goodarzi, M.S.; Kamyar, A.; Kazi, S.N. Boundary layer flow and heat transfer of FMWCNT/water nanofluids over a flat plate. *Fluids* **2016**, *1*, 31. [CrossRef]
4. Buongiorno, J. Convective Transport in Nanofluids. *J. Heat Transf.* **2006**, *128*, 240. [CrossRef]
5. Ho, C.J.; Chung, Y.N.; Lai, C.-M. Thermal performance of Al $_2$O$_3$/water nanofluid in a natural circulation loop with a mini-channel heat sink and heat source. *Energy Convers. Manag.* **2014**, *87*, 848–858. [CrossRef]
6. Kang, Z.; Wang, L. Effect of Thermal-Electric Cross Coupling on Heat Transport in Nanofluids. *Energies* **2017**, *10*, 123. [CrossRef]
7. Asirvatham, L.G.; Vishal, N.; Gangatharan, S.K.; Lal, D.M. Experimental study on forced convective heat transfer with low volume fraction of CuO/water nanofluid. *Energies* **2009**, *2*, 97–119. [CrossRef]
8. Patil, M.S.; Kim, S.C.; Seo, J.-H.; Lee, M.-Y. Review of the Thermo-Physical Properties and Performance Characteristics of a Refrigeration System Using Refrigerant-Based Nanofluids. *Energies* **2016**, *9*, 22. [CrossRef]
9. Patil, M.S.; Seo, J.-H.; Kang, S.-J.; Lee, M.-Y. Review on Synthesis, Thermo-Physical Property, and Heat Transfer Mechanism of Nanofluids. *Energies* **2016**, *9*, 840. [CrossRef]
10. Choi, S.U.S. Enhancing thermal conductivity of fluids with nanoparticles. *ASME-Publications-Fed* **1995**, *231*, 99–106.
11. Eastman, J.A.; Choi, U.S.; Li, S.; Thompson, L.J.; Lee, S. Enhanced thermal conductivity through the development of nanofluids. In *MRS Proceedings*; Cambridge University Press: Cambridge, UK, 1996; Volume 457, p. 3.
12. Eastman, J.A.; Choi, S.U.S.; Li, S.; Yu, W.; Thompson, L.J. Anomalously increased effective thermal conductivities of ethylene glycol-based nanofluids containing copper nanoparticles. *Appl. Phys. Lett.* **2001**, *78*, 718–720. [CrossRef]
13. Xuan, Y.; Li, Q. Heat transfer enhancement of nanofluids. *Int. J. Heat Fluid Flow* **2000**, *21*, 58–64. [CrossRef]
14. Choi, S.U.S.; Zhang, Z.G.; Yu, W.; Lockwood, F.E.; Grulke, E.A. Anomalous thermal conductivity enhancement in nanotube suspensions. *Appl. Phys. Lett.* **2001**, *79*, 2252–2254. [CrossRef]

15. Colangelo, G.; Favale, E.; de Risi, A.; Laforgia, D. Results of experimental investigations on the heat conductivity of nanofluids based on diathermic oil for high temperature applications. *Appl. Energy* **2012**, *97*, 828–833. [CrossRef]

16. Mintsa, H.A.; Roy, G.; Nguyen, C.T.; Doucet, D. New temperature dependent thermal conductivity data for water-based nanofluids. *Int. J. Therm. Sci.* **2009**, *48*, 363–371. [CrossRef]

17. Gu, B.; Hou, B.; Lu, Z.; Wang, Z.; Chen, S. Thermal conductivity of nanofluids containing high aspect ratio fillers. *Int. J. Heat Mass Transf.* **2013**, *64*, 108–114. [CrossRef]

18. Nnanna, A.G. Experimental model of temperature-driven nanofluid. *J. Heat Transf.* **2007**, *129*, 697–704. [CrossRef]

19. Beg, O.A.; Rashidi, M.M.; Akbari, M.; Hosseini, A. Comparative numerical study of single-phase and two-phase models for bio-nanofluid transport phenomena. *J. Mech. Med. Biol.* **2014**, *14*, 1450011. [CrossRef]

20. Bhatti, M.M.; Rashidi, M.M. Effects of thermo-diffusion and thermal radiation on Williamson nanofluid over a porous shrinking/stretching sheet. *J. Mol. Liq.* **2016**, *221*, 567–573. [CrossRef]

21. Sheikholeslami, M.; Rashidi, M.M. Effect of space dependent magnetic field on free convection of Fe_3O_4–water nanofluid. *J. Taiwan Inst. Chem. Eng.* **2015**, *56*, 6–15. [CrossRef]

22. Nkurikiyimfura, I.; Wang, Y.; Pan, Z. Heat transfer enhancement by magnetic nanofluids—A review. *Renew. Sustain. Energy Rev.* **2013**, *21*, 548–561. [CrossRef]

23. Zablotsky, D.; Mezulis, A.; Blums, E. Surface cooling based on the thermomagnetic convection: Numerical simulation and experiment. *Int. J. Heat Mass Transf.* **2009**, *52*, 5302–5308. [CrossRef]

24. Xuan, Y.; Li, Q.; Ye, M. Investigations of convective heat transfer in ferrofluid microflows using lattice-Boltzmann approach. *Int. J. Therm. Sci.* **2007**, *46*, 105–111. [CrossRef]

25. Rashidi, M.M.; Nasiri, M.; Khezerloo, M.; Laraqi, N. Numerical investigation of magnetic field effect on mixed convection heat transfer of nanofluid in a channel with sinusoidal walls. *J. Magn. Magn. Mater.* **2016**, *401*, 159–168. [CrossRef]

26. Bahiraei, M.; Hangi, M. Flow and heat transfer characteristics of magnetic nanofluids: A review. *J. Magn. Magn. Mater.* **2015**, *374*, 125–138. [CrossRef]

27. Yu, W.; Xie, H. A review on nanofluids: Preparation, stability mechanisms, and applications. *J. Nanomater.* **2012**, *2012*, 1. [CrossRef]

28. Wang, X.-Q.; Mujumdar, A.S. Heat transfer characteristics of nanofluids: A review. *Int. J. Therm. Sci.* **2007**, *46*, 1–19. [CrossRef]

29. Vo, T.Q.; Kim, B. Transport phenomena of water in molecular fluidic channels. *Sci. Rep.* **2016**, *6*. [CrossRef] [PubMed]

30. Kim, B.H.; Beskok, A.; Cagin, T. Viscous heating in nanoscale shear driven liquid flows. *Microfluid. Nanofluidics* **2010**, *9*, 31–40. [CrossRef]

31. Lomascolo, M.; Colangelo, G.; Milanese, M.; de Risi, A. Review of heat transfer in nanofluids: Conductive, convective and radiative experimental results. *Renew. Sustain. Energy Rev.* **2015**, *43*, 1182–1198. [CrossRef]

32. Sundar, L.S.; Sharma, K.V.; Naik, M.T.; Singh, M.K. Empirical and theoretical correlations on viscosity of nanofluids: A review. *Renew. Sustain. Energy Rev.* **2013**, *25*, 670–686. [CrossRef]

33. Iacobazzi, F.; Milanese, M.; Colangelo, G.; Lomascolo, M.; de Risi, A. An explanation of the Al_2O_3 nanofluid thermal conductivity based on the phonon theory of liquid. *Energy* **2016**, *116*, 786–794. [CrossRef]

34. Vo, T.Q.; Park, B.; Park, C.; Kim, B. Nano-scale liquid film sheared between strong wetting surfaces: Effects of interface region on the flow. *J. Mech. Sci. Technol.* **2015**, *29*, 1681–1688. [CrossRef]

35. Vo, T.Q.; Barisik, M.; Kim, B. Near-surface viscosity effects on capillary rise of water in nanotubes. *Phys. Rev. E* **2015**, *92*, 53009. [CrossRef] [PubMed]

36. Bocquet, L.; Charlaix, E. Nanofluidics, from bulk to interfaces. *Chem. Soc. Rev.* **2010**, *39*, 1073–1095. [CrossRef] [PubMed]

37. Bocquet, L.; Barrat, J.-L. Flow boundary conditions from nano-to micro-scales. *Soft Matter* **2007**, *3*, 685–693. [CrossRef]

38. Colangelo, G.; Favale, E.; Miglietta, P.; Milanese, M.; de Risi, A. Thermal conductivity, viscosity and stability of Al_2O_3-diathermic oil nanofluids for solar energy systems. *Energy* **2016**, *95*, 124–136. [CrossRef]

39. Sundar, L.S.; Farooky, M.H.; Sarada, S.N.; Singh, M.K. Experimental thermal conductivity of ethylene glycol and water mixture based low volume concentration of Al_2O_3 and CuO nanofluids. *Int. Commun. Heat Mass Transf.* **2013**, *41*, 41–46. [CrossRef]

40. Bishop, K.J.M.; Wilmer, C.E.; Soh, S.; Grzybowski, B.A. Nanoscale forces and their uses in self-assembly. *Small* **2009**, *5*, 1600–1630. [CrossRef] [PubMed]

41. Nkurikiyimfura, I.; Wang, Y.; Pan, Z. Effect of chain-like magnetite nanoparticle aggregates on thermal conductivity of magnetic nanofluid in magnetic field. *Exp. Therm. Fluid Sci.* **2013**, *44*, 607–612. [CrossRef]

42. Fang, X.; Xuan, Y.; Li, Q. Anisotropic thermal conductivity of magnetic fluids. *Prog. Nat. Sci.* **2009**, *19*, 205–211. [CrossRef]

43. Prasher, R.; Evans, W.; Meakin, P.; Fish, J.; Phelan, P.; Keblinski, P. Effect of aggregation on thermal conduction in colloidal nanofluids. *Appl. Phys. Lett.* **2006**, *89*, 143119. [CrossRef]

44. Philip, J.; Shima, P.D.; Raj, B. Evidence for enhanced thermal conduction through percolating structures in nanofluids. *Nanotechnology* **2008**, *19*, 305706. [CrossRef] [PubMed]

45. Fu, H.L.; Gao, L. Theory for anisotropic thermal conductivity of magnetic nanofluids. *Phys. Lett. A* **2011**, *375*, 3588–3592. [CrossRef]

46. Shima, P.D.; Philip, J. Tuning of thermal conductivity and rheology of nanofluids using an external stimulus. *J. Phys. Chem. C* **2011**, *115*, 20097–20104. [CrossRef]

47. Philip, J.; Shima, P.D.; Raj, B. Enhancement of thermal conductivity in magnetite based nanofluid due to chainlike structures. *Appl. Phys. Lett.* **2007**, *91*, 203108. [CrossRef]

48. Altan, C.L.; Elkatmis, A.; Yüksel, M.; Aslan, N.; Bucak, S. Enhancement of thermal conductivity upon application of magnetic field to Fe3O4 nanofluids. *J. Appl. Phys.* **2011**, *110*, 93917. [CrossRef]

49. Sheikholeslami, M.; Ganji, D.D. Nanofluid convective heat transfer using semi analytical and numerical approaches: A review. *J. Taiwan Inst. Chem. Eng.* **2016**, *65*, 43–77. [CrossRef]

50. Rajagopal, K.R.; Tao, L. *Mechanics of Mixtures*; Series on Advances in Mathematics for Applied Sciences; World Scientific Publishers: Singapore, 1995; Volume 35.

51. Massoudi, M. A note on the meaning of mixture viscosity using the classical continuum theories of mixtures. *Int. J. Eng. Sci.* **2008**, *46*, 677–689. [CrossRef]

52. Massoudi, M. A Mixture Theory formulation for hydraulic or pneumatic transport of solid particles. *Int. J. Eng. Sci.* **2010**, *48*, 1440–1461. [CrossRef]

53. Zhou, Z.; Wu, W.-T.; Massoudi, M. Fully developed flow of a drilling fluid between two rotating cylinders. *Appl. Math. Comput.* **2016**, *281*, 266–277. [CrossRef]

54. Slattery, J.C. *Advanced Transport Phenomena*; Cambridge University Press: Cambridge, UK, 1999.

55. Phillips, R.J.; Armstrong, R.C.; Brown, R.A.; Graham, A.L.; Abbott, J.R. A constitutive equation for concentrated suspensions that accounts for shear-induced particle migration. *Phys. Fluids A Fluid Dyn.* **1992**, *4*, 30–40. [CrossRef]

56. Tzou, D.Y. Thermal instability of nanofluids in natural convection. *Int. J. Heat Mass Transf.* **2008**, *51*, 2967–2979. [CrossRef]

57. Liu, I.-S. *Continuum Mechanics*; Springer Science & Business Media: Berlin, Germany, 2002.

58. Syam, S.L.; Singh, M.K.; Sousa, A.C.M. Investigation of thermal conductivity and viscosity of Fe_3O_4 nanofluid for heat transfer applications. *Int. Commun. Heat Mass Transf.* **2013**, *44*, 7–14. [CrossRef]

59. Sheikholeslami, M.; Rashidi, M.M.; Ganji, D.D. Effect of non-uniform magnetic field on forced convection heat transfer of–water nanofluid. *Comput. Methods Appl. Mech. Eng.* **2015**, *294*, 299–312. [CrossRef]

60. Song, D.; Jing, D.; Luo, B.; Geng, J.; Ren, Y. Modeling of anisotropic flow and thermodynamic properties of magnetic nanofluids induced by external magnetic field with varied imposing directions. *J. Appl. Phys.* **2015**, *118*, 45101. [CrossRef]

61. Kole, M.; Dey, T.K. Investigation of thermal conductivity, viscosity, and electrical conductivity of graphene based nanofluids. *J. Appl. Phys.* **2013**, *113*, 84307. [CrossRef]

62. Mehrali, M.; Sadeghinezhad, E.; Latibari, S.T.; Kazi, S.N.; Mehrali, M.; Zubir, M.N.B.M.; Metselaar, H.S.C. Investigation of thermal conductivity and rheological properties of nanofluids containing graphene nanoplatelets. *Nanoscale Res. Lett.* **2014**, *9*, 15. [CrossRef] [PubMed]

63. Maxwell, J.C. *A Treatise on Electricity and Magnetism*; Clarendon Press: Gloucestershire, UK, 1881; Volume 1.

64. Ganguly, S.; Sikdar, S.; Basu, S. Experimental investigation of the effective electrical conductivity of aluminum oxide nanofluids. *Powder Technol.* **2009**, *196*, 326–330. [CrossRef]

65. Shen, L.P.; Wang, H.; Dong, M.; Ma, Z.C.; Wang, H.B. Solvothermal synthesis and electrical conductivity model for the zinc oxide-insulated oil nanofluid. *Phys. Lett. A* **2012**, *376*, 1053–1057. [CrossRef]

66. Sarojini, K.G.K.; Manoj, S.V.; Singh, P.K.; Pradeep, T.; Das, S.K. Electrical conductivity of ceramic and metallic nanofluids. *Colloids Surfaces A Physicochem. Eng. Asp.* **2013**, *417*, 39–46. [CrossRef]

67. Aminfar, H.; Mohammadpourfard, M.; Mohseni, F. Two-phase mixture model simulation of the hydro-thermal behavior of an electrical conductive ferrofluid in the presence of magnetic fields. *J. Magn. Magn. Mater.* **2012**, *324*, 830–842. [CrossRef]

68. Minea, A.A.; Luciu, R.S. Investigations on electrical conductivity of stabilized water based Al_2O_3 nanofluids. *Microfluid. Nanofluidics* **2012**, *13*, 977–985. [CrossRef]

69. Malvandi, A. Film boiling of magnetic nanofluids (MNFs) over a vertical plate in presence of a uniform variable-directional magnetic field. *J. Magn. Magn. Mater.* **2016**, *406*, 95–102. [CrossRef]

70. Hahn, D.W.; Özişik, M.N. Heat Conduction Fundamentals. In *Heat Conduct*, 3rd ed.; John Wiley & Sons: New York, NY, USA, 2012; pp. 1–39.

71. Ozisik, M.N. *Boundary Value Problems of Heat Conduction*; Courier Corporation: North Chelmsford, MA, USA, 2013.

72. Massoudi, M. On the heat flux vector for flowing granular materials—Part I: Effective thermal conductivity and background. *Math. Methods Appl. Sci.* **2006**, *29*, 1585–1598. [CrossRef]

73. Massoudi, M. On the heat flux vector for flowing granular materials—Part II: Derivation and special cases. *Math. Methods Appl. Sci.* **2006**, *29*, 1599–1613. [CrossRef]

74. Reinecke, B.N.; Shan, J.W.; Suabedissen, K.K.; Cherkasova, A.S. On the anisotropic thermal conductivity of magnetorheological suspensions. *J. Appl. Phys.* **2008**, *104*, 23507. [CrossRef]

75. Nan, C.-W.; Birringer, R.; Clarke, D.R.; Gleiter, H. Effective thermal conductivity of particulate composites with interfacial thermal resistance. *J. Appl. Phys.* **1997**, *81*, 6692–6699. [CrossRef]

76. Li, J.; Huang, Y.; Liu, X.; Lin, Y.; Bai, L.; Li, Q. Effect of aggregates on the magnetization property of ferrofluids: A model of gaslike compression. *Sci. Technol. Adv. Mater.* **2007**, *8*, 448–454. [CrossRef]

77. Massoudi, M. On the importance of material frame-indifference and lift forces in multiphase flows. *Chem. Eng. Sci.* **2002**, *57*, 3687–3701. [CrossRef]

78. Nye, J.F. *Physical Properties of Crystals: Their Representation by Tensors and Matrices*; Oxford University Press: Oxford, UK, 1985.

79. Touloukian, Y.S.; Powell, R.W.; Ho, C.Y.; Nicolaou, M.C. *Thermophysical Properties of Matter—The TPRC Data Series. Volume 10. Thermal Diffusivity*; DTIC Document: Bedford, MA, USA, 1974.

80. Xie, H.; Wang, J.; Xi, T.; Liu, Y.; Ai, F.; Wu, Q. Thermal conductivity enhancement of suspensions containing nanosized alumina particles. *J. Appl. Phys.* **2002**, *91*, 4568–4572. [CrossRef]

81. Van den Brule, B. A network theory for the thermal conductivity of an amorphous polymeric material. *Rheol. Acta* **1989**, *28*, 257–266. [CrossRef]

82. Dai, S.C.; Tanner, R.I. Anisotropic thermal conductivity in sheared polypropylene. *Rheol. Acta* **2006**, *45*, 228–238. [CrossRef]

83. OpenCFD. *OpenFOAM Programmer's Guide Version 2.1.0*; OpenCFD, Ed.; Free Software Foundation, Inc.: Boston, MA, USA, 2011.

84. Gouin, H.; Saccomandi, G. Travelling waves of density for a fourth-gradient model of fluids. *Contin. Mech. Thermodyn.* **2016**, 1–13. [CrossRef]

85. Gărăjeu, M.; Gouin, H.; Saccomandi, G. Scaling Navier-Stokes equation in nanotubes. *Phys. Fluids* **2013**, *25*, 82003. [CrossRef]

86. Rusche, H. *Computational Fluid Dynamics of Dispersed Two-Phase Flows at High Phase Fractions*; Imperial College London (University of London): London, UK, 2002; Volume 1.

87. Wu, W.-T.; Massoudi, M.; Yan, H. Heat Transfer and Flow of Nanofluids in a Y-Type Intersection Channel with Multiple Pulsations: A Numerical Study. *Energies* **2017**, *10*, 492. [CrossRef]

88. Job, V.M.; Gunakala, S.R. Mixed convection nanofluid flows through a grooved channel with internal heat generating solid cylinders in the presence of an applied magnetic field. *Int. J. Heat Mass Transf.* **2017**, *107*, 133–145. [CrossRef]

89. Selimefendigil, F.; Öztop, H.F. Pulsating nanofluids jet impingement cooling of a heated horizontal surface. *Int. J. Heat Mass Transf.* **2014**, *69*, 54–65. [CrossRef]

90. Sridhara, V.; Satapathy, L.N. Al_2O_3-based nanofluids: A review. *Nanoscale Res. Lett.* **2011**, *6*, 456. [CrossRef] [PubMed]

91. Sheikholeslami, M.; Gorji-Bandpay, M.; Ganji, D.D. Magnetic field effects on natural convection around a horizontal circular cylinder inside a square enclosure filled with nanofluid. *Int. Commun. Heat Mass Transf.* **2012**, *39*, 978–986. [CrossRef]

92. Mahmoudi, A.H.; Pop, I.; Shahi, M. Effect of magnetic field on natural convection in a triangular enclosure filled with nanofluid. *Int. J. Therm. Sci.* **2012**, *59*, 126–140. [CrossRef]